



Study the Effect of Manganese Ions Doping on the Size- Strain of SnO₂ nanoparticles Using X-Ray Diffraction Data

Zahraa A. Kamil✉

Department of Physics, College of Education for
Pure Science Ibn-AL-Haitham, University of
Baghdad, Baghdad, Iraq.

Tagreed M. Al-Saadi*✉

Department of Physics, College of Education for
Pure Science Ibn-AL-Haitham, University of
Baghdad, Baghdad, Iraq.

*Corresponding Author: taghreed.m.m@ihcoedu.uobaghdad.edu.iq

Article history: Received 1 October 2022, Accepted 17 January 2023, Published in July 2023.

doi.org/10.30526/36.3.3052

Abstract

In this study, SnO₂ nanoparticles were prepared from cost-low tin chloride (SnCl₂.2H₂O) and ethanol by adding ammonia solution by the sol-gel method, which is one of the lowest-cost and simplest techniques. The SnO₂ nanoparticles were dried in a drying oven at a temperature of 70°C for 7 hours. After that, it burned in an oven at a temperature of 200°C for 24 hours. The structure, material, morphological, and optical properties of the synthesized SnO₂ in nanoparticle sizes are studied utilizing X-ray diffraction. The Scherrer expression was used to compute nanoparticle sizes according to X-ray diffraction, and the results needed to be scrutinized more closely. The micro-strain indicates the broadening of diffraction peaks for nanoparticles that are not ideal crystals. The extra broadening of the diffraction peak may lead to a miscalculation of the nanoparticle size. We use the Williamson-Hall method to directly compute and discuss the particle size and micro-strain of SnO₂ nanoparticles and compare them with results obtained using the Scherrer method. In conclusion, the straight line has been derived due to Williamson–Hall methods demonstrating the nanoparticles' uniformity.

Keywords: SnO₂, Williamson-Hall, X-ray diffraction, Nanoparticles, Structural Properties

1. Introduction

Many studies have been carried out intensively on wide band gap semiconductor materials over the last few years according to their potential use in various optical devices and physics applications [1]. Tin oxide SnO₂ is one of the most important IV–VI semiconductors; it is n-type, has a wide band gap material around 3.6–4.0 eV [2], and has a large exciton binding energy of 130 meV [3]. The metal oxide semiconductor SnO₂ has high chemical stability, low cost, high electron mobility, a long life, and a simple manufacturing technique [4]. Moreover, these characteristics make it a promising semiconductor material for different intriguing applications in technology [5]. The SnO₂ nanomaterial has gotten great interest in different fields lately because of its prospective



uses in gas sensors, catalytic, electrochemical, anodes in lithium batteries, optoelectronic devices, and biomedical applications due to its suitability, cost, high photosensitivity, and stability [6]. There are different techniques employed to synthesize and obtain the SnO₂ nanoparticles, such as thermal oxidation, the sol-gel procedure, chemical vapor deposition, and spray pyrolysis [7]. Novel physical features arising from size uniformity reduction and dispersion of SnO₂ are very important challenges for the present and future strategies of nanodevice applications in sensor, optical, and electronic fields [8]. Of the various methods mentioned that have the ability to produce large volumes of nanomaterial, the sol-gel method is the most simple, popular, inexpensive, and industrially applicable compared with other existing methods [9]. Nanometer-sized materials and semiconductor particles have unique features with a large potential for applications. Metal oxide semiconductors have been intensively used because of their low cost. Among the different metal oxide semiconductors, SnO₂ is attracting more attention since it has higher conduction and is transparent [10]. Since nanoscale tin oxide SnO₂ piqued curiosity, many researchers have devoted considerable efforts to synthesizing SnO₂ nanostructures with varied morphologies, such as nanoparticles, nanowires, nanorods, nanotubes, nanosheets, and 3D nanospheres [11]. To achieve defect-free nanoparticles, we must make efforts during the synthesis of nanoparticles since a crystal flaw will influence the attributes of the resultant nanostructure materials. The crystal materials become perfect when they have extended, indefinitely uniform configurations in directions. In fact, crystals aren't flawless because, as size expands, there is an eternal variation. The effect of divergence from crystalline perfectly can be shown from the altered diffraction peak's widening [12]. According to broadening, we can calculate the fundamental crystallite size and lattice strain. However, the size of the coherent diffraction domain has been measured by crystalline size. The contact or sinter stress, grain boundary stress, and nonlinear stress cause lattice strain and stacking faults, which measure the distribution of lattice constants for crystal imperfection. Bragg peaks were influenced by lattice strain and crystallite size, which increased peak width intensity with shifting peak locations. Crystal structure, mechanical characteristics (strain and stress), and lattice parameters are influenced by pre- and post-heating treatment in the Sol-gel method [13]. In the present work, the SnO₂ nanoparticle was prepared via a simple aqueous solution growth technique. The crystallite sizes for SnO₂, which are derived via X-ray diffraction, are using the W-H plotting approach while accounting for microstrain and compared with the mean particle sizes computed due to Scherrer's equation. Scherrer's equation has been used to compute crystallite size according to the adjusted line width.

2. Experimental Details

Tin dioxide nanoparticles were prepared using the sol-gel method as follows:

5.259 g of tin chloride (SnCl₄·5H₂O) was dissolved in 150 ml of deionized water while stirring continuously for 40 minutes. Then, 6 ml of ammonia (NH₃) was added to adjust the pH function while continuing to stir until it turned into a white gelatinous liquid. Using filter paper, the solution was filtered by continuous washing with distilled water. The sample was dried in a drying oven at 70°C for 7 hours. The sample was incinerated in an oven at 200°C for 24 hours. Finally, the material was ground with a ceramic mortar and converted into fine (nano) particles of SnO₂. The other sample doped with manganese ions was prepared by adding manganese nitrate in the same way at a molar ratio of 5%.

3. Results and Discussion

The crystallographic characterization of the synthesized structure material and phase purity of pure SnO₂ doped with Mn ions is done by using the XRD pattern technique. It reveals the rutile tetragonal structure of SnO₂ nanocrystals. The XRD diffraction of the sample showed that the top peaks were due to the complex of pure SnO₂ nanoparticles. It can be listed as a tetragonal structure. We can show and record five distinct tin oxide peaks and detect them due to the patterns in the range (10°–80°) assigned to the planes (110), (101), (111), (211), and (301). The diffraction peaks were assigned to the tetragonal structure of tin dioxide. The crystallographic structure suggests that it is unaffected by the doping sample. In **Table 2**, it can be noted that the lattice parameters and unit cell size increase after adding the Mn³⁺ ions to the samples of SnO₂ nanoparticles. The increase in the lattice parameters may be due to the smaller ionic radius of Mn³⁺ (0.65 Å) which was substituted in place of the Sn⁴⁺ (0.69 Å) site. The tin oxide phase didn't change. Lattice constants are computed according to Match!3 software. Results are shown in **Table 2**. However, the density of tin oxide is calculated for the samples using X-ray data with an expression [14, 15]:

$$\rho = \frac{N M_w}{N_A V} \quad (1)$$

Where, N , M_w , N_A and V are the number of atoms in the unit cell, molecule weight, Avogadro's number, and lattice volume. The results of the density calculation from the X-ray are noted in the table: the density decreases with impurity according to equation (1), it is inversely proportional to the size of the unit cell. The data in **Table 1** show agreement with the standard results.

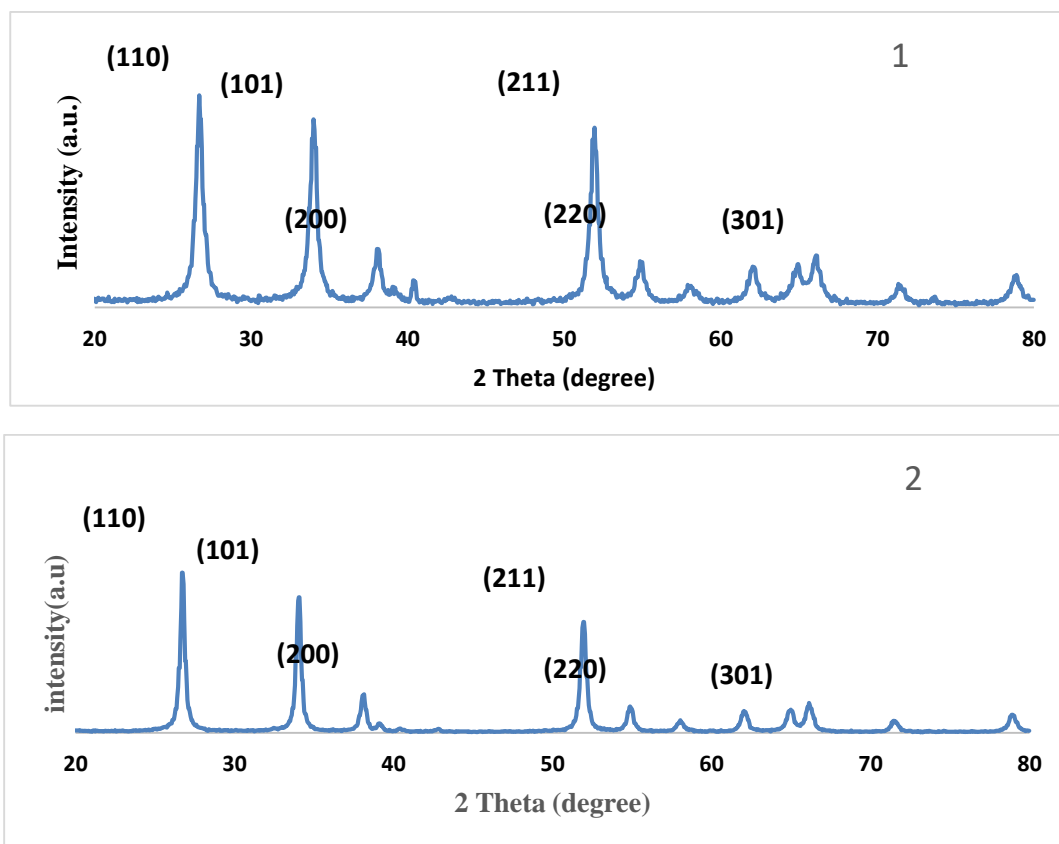


Figure 1. X- Ray diffraction of two samples of pure SnO₂ nanoparticles and doped with Mn.

Table 1. Lattice constant and density of SnO₂ nanoparticles.

Sample	lattice constant (Å)		Unit cell Volume (Å ³)	ρ (g/cm ³)
	a=b	c		
1	4.738	3.185	71.438	7.0028
2	4.737	3.202	71.850	6.9648

Crystallite Size and Strain

Scherer Method

X-ray data were used for correlation peaks with crystallite size and lattice strain due to the dislocations [16] and vacancies [17]. The crystallite size of SnO₂ nanoparticles can be determined using the Scherer equation with the extension method of the X-ray line that is given by [18, 19].

$$FWHM = \frac{K\lambda}{D \cdot \cos\theta} \quad (2)$$

Where FWHM is the full width of the diffraction peak at half-maximum, K denotes the shape factor $\cong 0.89$, $\lambda = 0.15406$ nm, D is the crystallite size and θ denotes the x-ray incident angle..

Crystal defects are caused by peak broadening that's caused by lattice strain and crystallite size. Peak broadening is related to the size of crystallites inversely; it is the result of a mix of instrumental effects and sample dependent. Using the connection, the FWHM corresponding to the tin oxide diffraction peak is calculated using the following equation [20].

$$FWHM = \beta_{measured}^2 + \beta_{instrumental}^2 \quad (3)$$

Williamson Hall Uniform Deformation Model (UDM)

However, it can get a good rough estimation of crystallite size according to the Scherrer equation. Moreover, the precision of this method is well known, but it overlooks the microstrain and its effect on the diffraction pattern. It can benefit from the analysis of Williamson-Hall [21]. The Williamson-Hall plot method is used to evaluate the change in crystallite size and strain as a function of angle [20]. According to the Williamson-Hall procedures, the contribution of Bragg's individual to line enlargement is given as [22–24]:

$$\beta \cos\theta = \frac{k\lambda}{D} + 4 \epsilon \sin\theta \quad (4)$$

Where (D) is the crystallite size of an X-ray diffraction peak, (β_D) and (β_ϵ) are the contributions of crystallite size and the strain to the expansion of the peak. In Eq. 2, on the inside, the strain was assumed to be uniform in all crystal directions, implying a model of uniform deformation. The crystallite size is determined to indicate the strain depending on the slope of the fitting line [25]. **Figure (2)** shows $\sin \theta$ plots with $\beta \cos\theta$ to find the results of uniform deformation Where K is 0.94 and λ the wavelength at the target = 1.5406 Å.

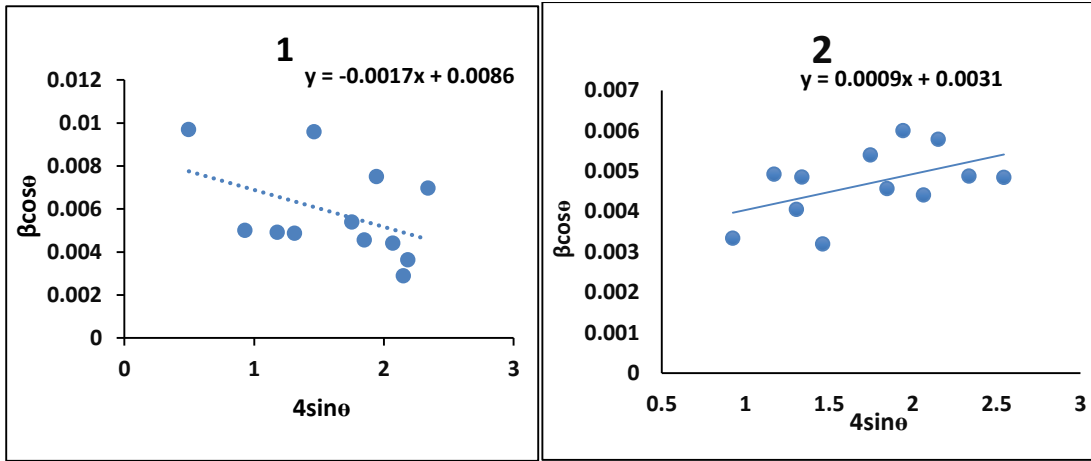


Figure 2. UDM analysis of pure SnO₂ nanoparticles and doped with Mn.

Depending on Hooke's law, the stress σ is linear proportional to strain ϵ at elastic limit and can be calculated using [25].

$$Y = \frac{\sigma}{\epsilon} \tag{5}$$

Where, Y is a Young's modulus in the (hkl) planes. We assume the lattice deformation stress is to be uniform. As a result, in the second component of the equation, this is reduced to modify Eq. (4) to give [22]:

$$\beta \cos \theta = \frac{k\lambda}{D} + \frac{4\sigma \sin \theta}{Y} \tag{6}$$

The relation between $\frac{4\sin\theta}{Y}$ and $\beta \cos \theta$ is linear and reduces to stress σ [26]. Elasticity modulus relates to the elastic compliances A_{ij} at semiconductor nanoparticles according to equation [27]:

$$\frac{1}{Y} = A_{11} - \frac{(k^2l^2 + l^2h^2 + h^2k^2)(2A_{11} - 2A_{12} - A_{44})}{(h^2 + k^2 + l^2)} \tag{7}$$

Where the elastic compatibilities are given by

$$A_{11} = \frac{(a_{11} + a_{12})}{(a_{11} - a_{12})(a_{11} + 2a_{12})}, A_{12} = \frac{(-a_{12})}{(a_{11} - a_{12})(a_{11} + 2a_{12})}, \text{ and } A_{44} = \frac{1}{a_{44}}$$

The elastic compliance is estimated according to the experimental values of the elastic constants a_{11} , a_{12} and a_{44} , and equal to 316 GPa, 56 GPa and 115 GPa [28].

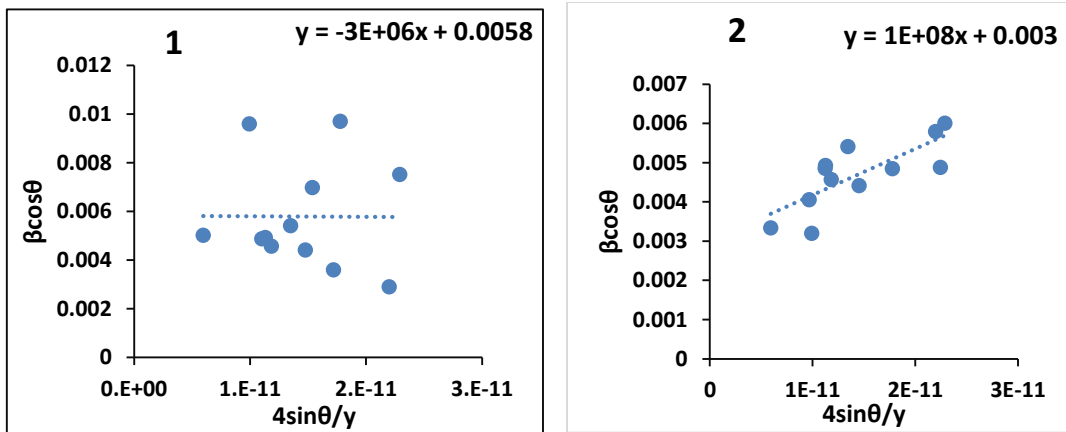


Figure 3. The USDm analysis of pure SnO₂ nanoparticles and doped with Mn.

The energy density model (EDM)

However, the crystal size, stress parameters, and strain are calculated using the energy density and uniform deformation. Under this assumption, the crystals are defined in Eq.(4) and considered homogeneous and isotropic. In general, the energy density U is considered independent and can be determined from the relationship (5)[29]:

$$U = \frac{1}{2} \epsilon^2 Y \tag{8}$$

Inserting Eq.(8) in Eq.(6) to get the energy relation and strain utilizing by relation [27, 28].

$$\beta \cos \theta = \frac{k\lambda}{D} + (4 \sin \theta (\frac{2U}{Y})^{1/2}) \tag{9}$$

Figure (4) indicate the plots between the $4 \sin \theta (\frac{2U}{Y})^{1/2}$ and $\beta \cos \theta$.

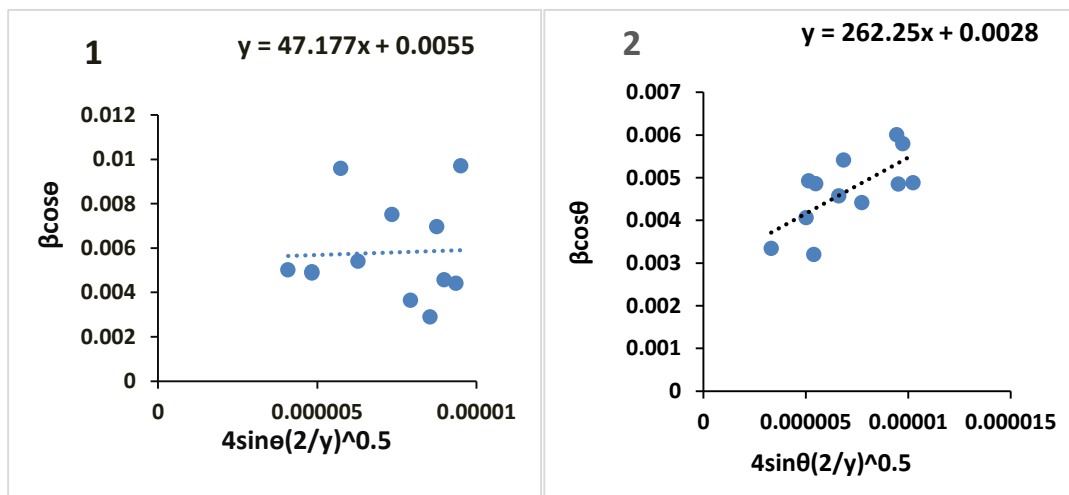


Figure 4. The UDEDM analysis of pure SnO₂ nanoparticles and doped with Mn.

Size-Strain Plot Model

Due to the isotropic nature of the crystals, the Lorentzian and Gaussian functions are used to define crystallite size and strain [30]. The linear relation between $(d\beta \cos \theta)^2$ as a function of $d^2 \beta \cos \theta$ is given by [27]

$$(d\beta \cos \theta)^2 = \frac{K}{D} (d^2 \beta \cos \theta) \left(\frac{\epsilon}{2}\right)^2 \tag{10}$$

The strain and crystallite size are determined using the linear fit of the supplied results data and plotted $(d\beta \cos \theta)^2$ as a function of $d^2 \beta \cos \theta$ and the y-intercept, as shown in **Figure 5**.

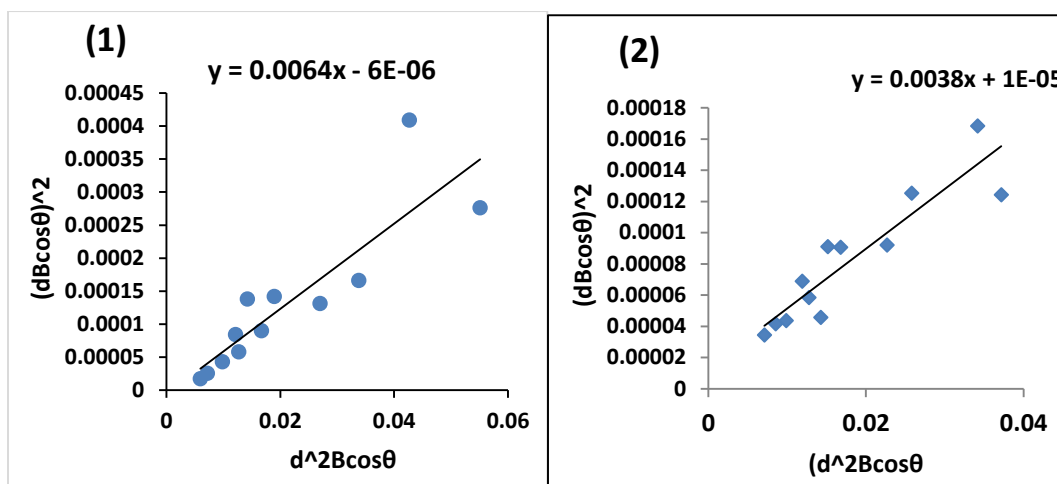


Figure 5. The SSP analysis of pure SnO₂ nanoparticles doped with Mn.

Table 3. The results of D, ε, and other factors calculated from different models.

Sample	Scherer	UDM		USDM			UEDDM			SSP		
	D (nm)	W-H D (nm)	ε x10 ⁻⁵	W-H D (nm)	ε x10 ⁻⁵	σ x10 ⁷ Pa	W-H D (nm)	ε x10 ⁻⁵	σ x10 ⁶ Pa	U kJ.m ⁻³	D (nm)	ε x10 ⁻³
1	16	1.39	3.1	23.90	2.27	10	25.20	1.298	17.14	22.23	21.66	4.90
2	44	1.38	3.1	46.22	7.57	10	49.52	10.21	134.77	68.78	36.49	6.32

4. Conclusion

The structure of SnO₂ nanoparticles has been synthesized by sol-gel autocombustion. In conclusion, the X-ray diffraction technique and Scherer equation employed in the characteristics of crystals and nanomaterials could result in inaccurate particle size determinations. Williamson-Hall models have been introduced as a good tool for dealing with nanomaterials because they describe the microstructure and show micro-strain and particle size. The system of Williamson-Hall is effective in accurately measuring stress, strain, crystal size, and energy density based on UDM, USDM, UEDDM, and SSP. It can suggest the Williamson-Hall model is more useful to understand crystal refinement.

References

1. Wong, M. H.; Bierwagen, O.; Kaplar, R. J.; Umezawa, H. Ultrawide-bandgap semiconductors: An overview. *Journal of Materials Research*, **2021**, *23*, 1-15.
2. Li, Z.; Sun, L.; Liu, Y.; Zhu, L.; Yu, D.; Wang, Y.; Yu, M.; SnSe@ SnO₂ core-shell nanocomposite for synchronous photothermal-photocatalytic production of clean water. *Environmental Science: Nano*, **2019**, *6*, 1507-1515.
3. Sabri, N. S.; Deni, M. S. M.; Zakaria, A.; Talari, M. K., Effect of Mn doping on structural and optical properties of SnO₂ nanoparticles prepared by mechanochemical processing. *Physics Procedia*, **2012**, *25*, 233-239.
4. Sabri, N. A.; Al-Agealy, H. J., Theoretical studies of electronic transition characteristics of sensitizer molecule dye N3-SnO₂ semiconductor interface. In *AIP Conference Proceedings*, **2022**, *37*, 1-23, 020062). AIP Publishing LLC.

5. Huang, Z.; Zhu, J.; Hu, Y.; Zhu, Y.; Zhu, G.; Hu, L.; Huang, W. Tin Oxide (SnO₂) Nanoparticles: Facile Fabrication, Characterization, and Application in UV Photodetectors. *Nanomaterials*, **2022**, *12*, 4, 63-75.
6. Nipa, S. T.; Akter, R.; Raihan, A.; Rasul, S. B.; Som, U.; Ahmed, S.; Rahman, W., State-of-the-art biosynthesis of tin oxide nanoparticles by chemical precipitation method towards photocatalytic application. *Environmental Science and Pollution Research*, **2022**, *23*, 1-23.
7. Chand, P.; Gaur, A.; Kumar, A., Structural and optical properties of ZnO nanoparticles synthesized at different pH values. *Journal of alloys and compounds*, **2012**, *539*, 174-178.
8. Mishra, M. K.; Singh, N.; Pandey, V.; Haque, F. Z.; Synthesis of SnO₂ nanoparticles and its application in sensing ammonia gas through photoluminescence. *Journal of Advanced Physics*, **2016**, *5*, 8-12.
9. Bokov, D.; Turki Jalil, A.; Chupradit, S.; Suksatan, W.; Javed Ansari, M.; Shewael, I. H.; Kianfar, E., Nanomaterial by sol-gel method: synthesis and application. *Advances in Materials Science and Engineering*, **2021**, *12*, 23-34
10. Balakrishnan, K.; & Murugasean, N., Synthesis and characterization of SnO₂ nanoparticles by co-precipitation method. *International Journal of Nano Dimension*, **2021**, *12*(1), 76-82.
11. Zhao, Q.; Ma, L.; Zhang, Q.; Wang, C.; Xu, X., SnO₂-based nanomaterials: synthesis and application in lithium-ion batteries and supercapacitors. *journal of Nanomaterials*, **2015**, *12*, 23-33
12. Motevalizadeh, L.; Heidary, Z.; Abrishami, M. E., Facile template-free hydrothermal synthesis and microstrain measurement of ZnO nanorods. *Bulletin of materials science*, **2014**, *37*, 397-405.
13. Mohaideen, H. M.; Fareed, S. S.; Natarajan, B.; Role of calcination temperatures on the structural and optical properties of NiO nanoparticles. *Surface Review and Letters*, **2019**, *26*, 1950043.
14. Mustafa, H. J.; Al-Saadi, T. M.; Effects of Gum Arabic-Coated Magnetite Nanoparticles on the Removal of Pb Ions from Aqueous Solutions. *Iraqi Journal of Science*, **2021**, *11*, 889-896.
15. Hussain, F. I.; Synthesis of Nano Compound (Ba_{1-x}Sr_xTiO₃) by Sol-Gel Method and Study its Structural Properties. *Ibn Al-Haitham Journal For Pure and Applied Sciences*, **2016**, *29*, 34-45.
16. Yogamalar, R.; Srinivasan, R.; Vinu, A.; Ariga, K.; Bose, A. C.; X-ray peak broadening analysis in ZnO nanoparticles. *Solid State Communications*, **2009**, *149*, 1919-1923.
17. Maniammal, K.; Madhu, G.; Biju, V.; X-ray diffraction line profile analysis of nanostructured nickel oxide: shape factor and convolution of crystallite size and microstrain contributions. *Physica E: Low-dimensional Systems and Nanostructures*, **2017**, *85*, 214-222.
18. Al-Saadi, T. M.; Jihad, M. A.; Preparation of graphene flakes and studying its structural properties. *Iraqi Journal of Science*, **2016**, *57*, 145-153.

19. Al-Saadi, T. M.; Abed, A. H.; Salih, A. A.; Synthesis and Characterization of AlyCu_{0.15}Zn_{0.85}-yFe₂O₄ Ferrite Prepared by the Sol-Gel Method. *Int. J. Electrochem. Sci*, **2018**, *13*, 8295-8302.
20. Yasmeen, S.; Iqbal, F.; Munawar, T.; Nawaz, M. A.; Asghar, M.; Hussain, A.; Synthesis, structural and optical analysis of surfactant assisted ZnO–NiO nanocomposites prepared by homogeneous precipitation method. *Ceramics International*, **2019**, *45*, 17859-17873.
21. Ebnalwaled, A. A.; Abd El-Raady, A. A.; Abo-Bakr, A. M.; On the effect of complexing agents on the structural and optical properties of cds nanocrystals. *Chalcogenide Letters*, **2013**, *10*, 55-62.
22. Biju, V.; Sugathan, N.; Vrinda, V.; Salini, S. L.; Estimation of lattice strain in nanocrystalline silver from X-ray diffraction line broadening. *Journal of materials science*, **2008**, *43*, 1175-1179.
23. Al-Kalifawi, E. J.; Al-Obodi, E. E.; Al-Saadi, T. M.; Characterization of Cr₂O₃ nanoparticles prepared by using different plant extracts. *Acad. J. Agric. Res*, **2018**, *6*, 26-32.
24. Al-Saadi, T. M.; Alsaady, L. J.; Preparation of Silver Nanoparticles by Sol-Gel Method and Study their Characteristics. *Ibn AL-Haitham Journal For Pure and Applied Science*, **2015**, *28*, 44-65
25. Geetha, M. S.; Nagabhushana, H.; Shivananjaiah, H. N.; Green mediated synthesis and characterization of ZnO nanoparticles using Euphorbia Jatropa latex as reducing agent. *Journal of Science: Advanced Materials and Devices*, **2016**, *1*, 301-310.
26. Thandavan, T. M. K.; Gani, S. M. A.; Wong, C. S.; Nor, R. M.; Evaluation of Williamson–Hall strain and stress distribution in ZnO nanowires prepared using aliphatic alcohol. *Journal of Nondestructive Evaluation*, **2015**, *34*, 1-9.
27. Al Boukhari, J.; Khalaf, A.; Awad, R.; Structural analysis and dielectric investigations of pure and rare earth elements (Y and Gd) doped NiO nanoparticles. *Journal of Alloys and Compounds*, **2020**, *820*, 153381.
28. Madhu, G.; Bose, V. C.; Maniammal, K.; Raj, A. A.; Biju, V.; Microstrain in nanostructured nickel oxide studied using isotropic and anisotropic models. *Physica B: Condensed Matter*, **2013**, *421*, 87-91.
29. Alani, A. T.; Al-Saadi, T. M.; X-ray analysis by williamson-hall methods of pure and doped ZnO nanoparticles. *Annals of the Romanian Society for Cell Biology*, **2021**, *23*, 6836-6845.
30. Irfan, H.; Racik K, M.; Anand, S.; Microstructural evaluation of CoAl₂O₄ nanoparticles by Williamson–Hall and size–strain plot methods. *Journal of Asian Ceramic Societies*, **2018**, *6*, 54-62.